Available online at www.sciencedirect.com
ScienceDirect
Journal of Hazardous Materials 159 (2008) 169–176
Journal of Hazardous Materials
www.elsevier.com/locate/jhazmat

Molecular simulation studies of adsorption of hydrogen cyanide and methyl ethyl ketone on zeolite NaX and activated carbon

R.R. Kotdawala, Nikolaos Kazantzis *, Robert W. Thompson

Department of Chemical Engineering, Worcester Polytechnic Institute, Worcester, MA 01609, USA

Received 7 January 2008; accepted 11 January 2008
Available online 19 January 2008

Abstract

In the present research study the primary aim is to understand and characterize the physical adsorption of polar molecules namely, hydrogen cyanide and methyl ethyl ketone (MEK) in zeolite NaX, and activated carbon through detailed Monte–Carlo simulations and computational quantum chemistry techniques. The sorption capacity and affinity of the zeolite is compared with activated carbon with different acid site concentrations, type of acid site, and pore sizes by simulating single component isotherms and Henry's constant at 25 °C. The role/contribution of certain types of electrostatic interactions namely charge–dipole, charge–induced dipole with zeolite NaX and activated carbon, as well as dipole–dipole interactions among polar molecules is analyzed and discussed.

Keywords: Hazardous molecules; Adsorption; Molecular modeling; Molecular simulation; Hydrogen cyanide; Methyl ethyl ketone

1. Introduction

Methyl ethyl ketone (MEK) is used as a solvent for gums, resins, and cellulose nitrate, as well as in consumer products such as lacquers, varnishes, paint remover, and glues [1,2]. Typically, it is exposed to air by gases emitted from the pertinent manufacturing industries producing the abovementioned products, or it is directly discharged in wastewater. It should be pointed out, that an exposure of 200 ppm of MEK causes irritation to the eyes, nose (mucous membranes) and throat. In addition to this, high MEK levels are associated with smog formation due to photochemical reactions with olefinic hydrocarbons [2,3]. In light of the above considerations and the hazardous nature of MEK under certain conditions, adsorption is considered to be one of the most preferable and operationally advantageous methods to effectively remove MEK from industrial gases especially using activated carbon and zeolites as adsorbents [2].

Following the above line of research, Yen and Jeng [2] carried out vapor phase adsorption experiments on zeolite Y and ZSM-5 of different Si/Al ratios varying from 5 to 31, where the concentration of MEK in the vapor phase was in the range of 100–1500 ppm. In this particular study, Zeolite Y was found to be more effective than ZSM-5 in removing MEK from air stream. Monneyron et al. [4] conducted vapor phase single component and binary component (with toluene and 1,4-dioxane) adsorption experiments on zeolite Y and ZSM-5. It was found that the component having the higher molecular weight adsorbed preferentially over the other, except in the case of MEK-toluene mixture adsorption on ZSM-5, where toluene was believed to be excluded due to steric effects. Pires et al. [5] studied the effect of dealumination of zeolite Na–Y on the sorption of MEK at 298 K, and showed that an increase in the percentage of dealumination reduced MEK adsorption, suggesting that sodium cations favor MEK. Uguina et al. [6] studied MEK desorption from silicalite and activated carbon beds, and suggested that the regeneration temperature for silicalite was in the range of 90–170 °C, whereas in the case of activated carbon it was found to be within the range of 150–240 °C. These findings suggest that dispersion interactions might be dominant in the case of silicalite, and electrostatic interactions might be the dominant ones in the case of activated carbon due to the presence of acid sites. Despite the aforementioned research efforts, the experimental data available in the pertinent body of literature are not currently adequate to understand the mechanism of MEK

* Corresponding author. Tel.: +1 508 8315666.
E-mail address: nikolas@wpi.edu (N. Kazantzis).

0304-3894/$ – see front matter © 2008 Elsevier B.V. All rights reserved.
doi:10.1016/j.jhazmat.2008.01.045

adsorption in activated carbons and zeolites, especially at the molecular level. Motivated by the above realization, one of the objectives of the present research study is to enhance our understanding and characterize the adsorption properties of MEK by focusing specifically on the effect of sodium cations in zeolite Y, as well as hydroxyl, carbonyl and carboxylic sites in activated carbon on the adsorption capacity of MEK using molecular simulation methods.

Furthermore, and in a conceptually similar methodological framework, the adsorption of hydrogen cyanide (HCN) will be studied as well, recognizing the fact that it represents an acutely poisonous compound, which might enter the human body by breathing contaminated air. The HCN vapors are commonly released to the air from various sources, including vehicle exhaust emissions, chemical processing, extraction of gold and silver from low grade ores, metal plating, steel, iron, and finishing industries, petroleum refineries, and waste disposed of in landfills. Currently, the best-known adsorbents for the removal of HCN from air are metal salt-impregnated activated carbons [7]. Freeman and Reucroft [7] and Reucroft et al. [8] studied the adsorption of HCN and the mixture of HCN-water on BPL activated carbon, a granular activated carbon supplied by Calgon Carbon Inc. The experimental results suggested that, adsorption of HCN strongly dominates over water, and HCN discourages additional adsorption of water vapor, which might be attributed to the greater polarizability and dipole moment of HCN.

In another study of the removal of HCN from air by Oliver et al. [9], copper containing and copper free synthetic activated carbons produced from porous sulfonated styrene/divinylbenzene resin were studied for assessing the removal efficiency of HCN. The prepared adsorbent performance was comparable to ASC Whetlerite carbons that contain salts of chromium, copper, and silver. Incorporation of copper into the starting material significantly increased HCN breakthrough times, but decreased the surface area and pore volume of the adsorbent. The results of X-ray photoelectron spectroscopy (XPS) analysis revealed partial or complete reduction of the starting divalent copper on the surface of the adsorbents, amply confirmed by the lack of formation of $(CN)_2$ during the adsorption of HCN, while the use of conventional Whetlerite carbon produced poisonous $(CN)_2$ gas. However, detailed and good-quality experimental data on the sorption of HCN from flue gases are limited, and do not suggest any suitable adsorbents to remove HCN. To elucidate the above phenomenon and identify proper adsorbents, in the present research study we also examine the sorption characteristics of zeolite NaX and activated carbon for HCN using molecular simulation methods.

The present paper is organized as follows: Section 2 provides a brief description of the particular molecular modeling approaches used, followed by a succinct description of the molecular simulation methods employed in the present study. Section 4 encompasses the study's main results along with a detailed discussion on the primary research findings. Finally, a few concluding remarks are provided in Section 5.

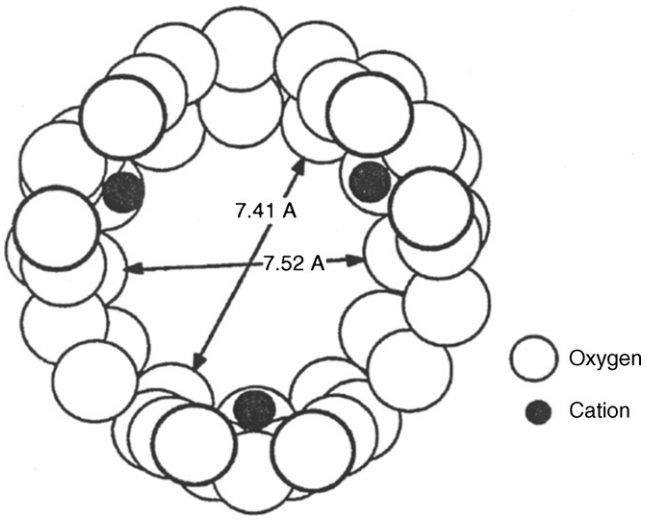

Fig. 1. Cross-section of a zeolite NaX adsorption cavity [11].

2. Molecular model description

2.1. Zeolite NaX model

Zeolite NaX was modeled by considering the zeolite cavity as spherically shaped with sodium cations located uniformly in the cavity [10,11] (Fig. 1). The specific locations of the sodium cations were taken from Karavias [11]. Moreover, the interactions with the spherical cavity were calculated using a spherically averaged potential for the dispersion and repulsion given by Karavias [11]:

$$\psi^{\text{disp}} = 4C\varepsilon_{1s}\left[\left(\frac{\sigma_{1s}}{R}\right)^{12} L\left\{\frac{r^2}{R^2}\right\} - \left(\frac{\sigma_{1s}}{R}\right)^{6} M\left\{\frac{r^2}{R^2}\right\}\right] \quad (1)$$

where

$$L\{x\} = \frac{1 + 12x + 25.2x^2 + 12x^3 + x^4}{(1-x)^{10}} \quad (2)$$

$$M\{x\} = \frac{1+x}{(1-x)^4} \quad (3)$$

with $x = r/R$ and ψ^{disp} being a function of r, the radial distance of the adsorbed molecule from the center of the cavity. The cavity radius, R, was chosen as the distance from the center to the nearest oxygen atom. For zeolite NaX, R is 7.057 Å [11]. In the above expression, $C\varepsilon_{1s}$ and σ_{1s} are the Lennard–Jones energy and colli-

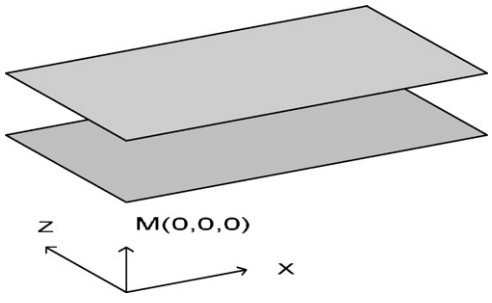

Fig. 2. Schematic diagram of a slit pore with origin at $M(0, 0, 0)$ [14].

sion diameter of molecule i with the solid wall, respectively. The interactions of the hazardous molecules of interest with sodium cations are mainly cation–induced dipole and cation–quadrupole moment interactions which can be calculated using Eqs. (4) and (5), respectively, as shown below [12]:

$$\psi^{\text{ind}} = -\frac{\alpha q^2}{2r^4(4\pi\varepsilon_0)^2} \tag{4}$$

where α is the polarizability of the molecule, q the electronic charge of the ion on the surface, ε_0 the permittivity of vacuum, and r is the distance between the centers of the interacting pair [12]. Notice, that interactions between the ion field and the point dipole are given by Yang [12]:

$$\psi^{\text{dipole}} = -\frac{q\mu\ \cos\ \theta}{r^2(4\pi\varepsilon_0)} \tag{5}$$

where μ is the dipole moment of the molecule, and θ is the angle between the direction of the field and the axis of the dipole.

The total interactions between HCN/MEK molecules and the zeolite cavity can be calculated as follows:

$$\psi_{\text{fw}} = \psi^{\text{disp}} + \psi^{\text{ind}} + \psi^{\text{dipole}} \tag{6}$$

It should be pointed out, that two types of interactions are considered in the present study, namely dispersion interactions and dipole–dipole interactions given by Eqs. (4) and (5). The following adsorbate (i)–adsorbate (j) interactions also were considered [13,14]:

$$U_{ij}^{\mu\mu} = \frac{\mu_i\mu_j}{r^3}(\sin\ \theta_i\ \sin\ \theta_j\ \cos\ \phi_{ij} - 2\cos\ \theta_i\ \cos\ \theta_j) \tag{7}$$

$$U_{ij}^{\text{disp}}(r) = \left[-\frac{1}{(4\pi\varepsilon_0)^2 r_{ij}^6}\left(\frac{3\alpha_i\alpha_j(I_i + I_j)}{I_i I_j 4}\right)\right] \tag{8}$$

where I_i and I_j are the first ionization potentials for molecules i and j, respectively.

2.2. Activated carbon model

The pores of activated carbon were modeled by considering two parallel walls, each of which comprises an infinite number of layers of graphite (Fig. 2). The graphite layers are composed of Lennard–Jones sites, but these are smeared out uniformly over each layer. The interaction between an adsorbate molecule and this smooth carbon surface is represented by the 10-4-3 potential [14]. Three types of polar surface sites: hydroxyl (H), carboxyl (C), and carbonyl (Ca) groups, were considered in the simulations, and are represented schematically in Fig. 3. The carboxyl, hydroxyl, and carbonyl sites can be considered as a collection of five, two and three point charges. The parameters (size of charge atom and partial charge) of point charges and their positions were taken from Jorge et al. [15,16]. Fig. 4 describes the type of site, number of sites, and their distributions. Each site was placed at 5 Å apart from its neighbor site (Fig. 4), and a symbol is assigned to each type of configuration. Moreover, Ca, H, and C refer to carbonyl, hydroxyl, and carboxyl sites, respectively. The number in the symbol represents the total number of sites in the pore. The single digit indicates that half of the sites are on each plate, while the double digit indicates that sites are located on a single plate. The cross-species parameters were calculated using the Lorentz–Berthelot combining rule [14–17]. As mentioned earlier, the electrostatic interactions namely charge–induced dipole moment and charge–quadrupole moment were calculated using Eqs. (4) and (5), respectively.

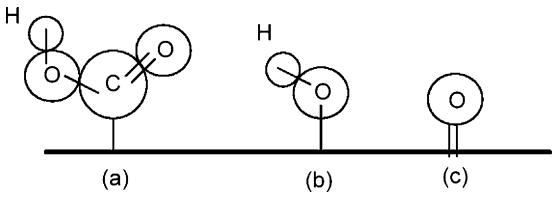

Fig. 3. Schematic representation of the surface sites on carbon: (a) a carboxyl group, (b) a hydroxyl group, and (c) a carbonyl group [15,16].

3. Simulation methods

We calculated adsorption isotherms using grand canonical Monte–Carlo (GCMC) simulations, in which the temperature (T), volume (V), and chemical potentials (μ) were kept constant. The algorithm for GCMC simulations is well documented [11], and we used the general methodology. The pressure (P) was calculated from the chemical potential and the equation of state for an ideal gas, and all simulations were performed in equilibrium bulk gas temperature of 298 K. Each type of Monte–Carlo trial (creation, destruction, and displacement/rotation) was chosen

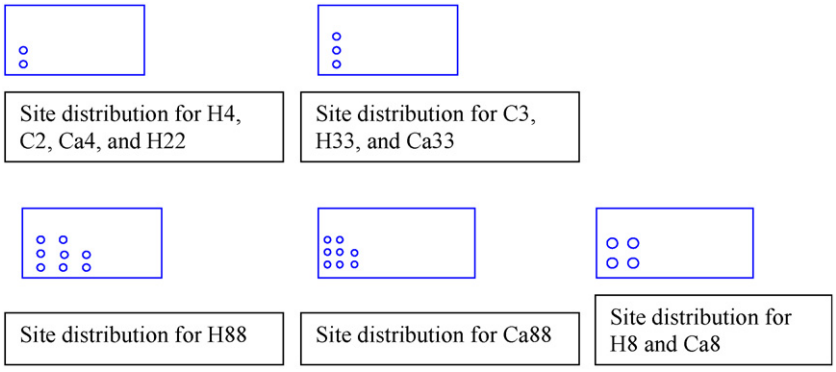

Fig. 4. Schematic diagram of different site distributions in activated carbon.

randomly with the same probability. The number of equilibrium steps in the simulations varied according to the operating conditions, in the range of 30–70 million. To calculate statistical uncertainties, simulations were divided into five blocks of trials (each varied from 5 to 12 million) and the observed standard deviation of block average was within 5%. During the sampling period, typical configurations for each run were stored in files and then converted into images. In the case of zeolite NaX, the interactions with molecules in four neighboring cavities also were considered. The molecules in the neighboring cavities were the images of molecules in the central cavity. In the case of activated carbon slit pores, the size of the simulation box was 3 nm × 1.5 nm × 3 nm.

We used rectangular simulation cells, bound in the *y*-direction by pore walls and replicated in *x*- and *z*-directions using periodic boundary conditions. In order to account for the long-range interactions, especially charge–dipole, charge–induced dipole, and dipole–dipole interactions, the interactions of molecules in the central cavity with neighboring cavities were considered.

4. Results and discussion

4.1. Sorption of hydrogen cyanide

Fig. 5 shows Henry's constant (*H*) for different carbonyl sites at 298 K. The Henry's law constant (*H*) values were in the range of 3–40 μg/g Pa. The heat of adsorption (*Q*) in the zero pressure limit for carbonyls sites were in the range of 10–35 kJ/mol (Fig. 6). Values of *H* and *Q* were greater in the case of Ca22 than that of Ca2. This difference is attributed to the relative distance between two sites of 5 Å in case of Ca22 as compared to 15 Å in Ca2. Fig. 7 shows the *H* values for different hydroxyl sites and zeolite NaX. *H* values for hydroxyls were in the range of 2–100 μg/g Pa and for zeolite NaX was 600 μg/g Pa, implying that zeolite NaX has a very high affinity for the HCN molecule. However, *Q* values were in the range of 15–40 kJ/mol (Fig. 8). Figs. 9 and 10 represent the *H* and *Q* values for activated carbon with different carboxyl sites. H values for carboxyls were in the range of 5–180 μg/g Pa, which is greater than that of hydroxyls and carbonyls. *Q* values were in the range of 15–45 kJ/mol for carboxyls.

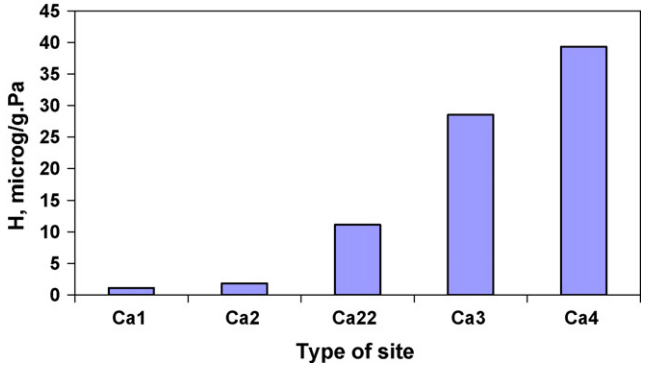

Fig. 5. Henry's law constant, *H*, for different carbonyl sites at 298 K.

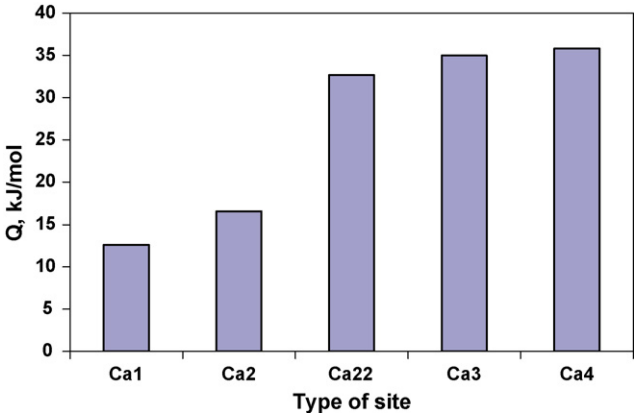

Fig. 6. Heat of adsorption, *Q*, for different carbonyl sites at 298 K.

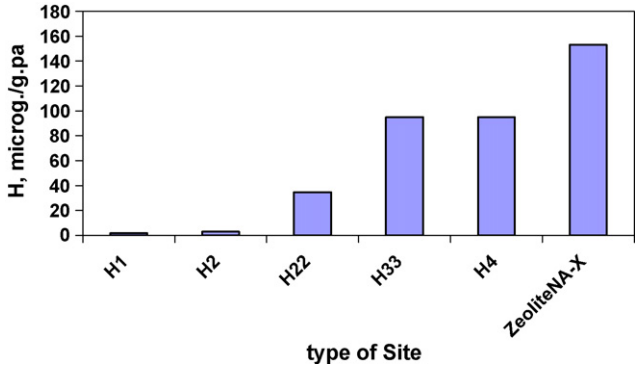

Fig. 7. Henry's law constant, *H*, for different hydroxyl sites at 298 K.

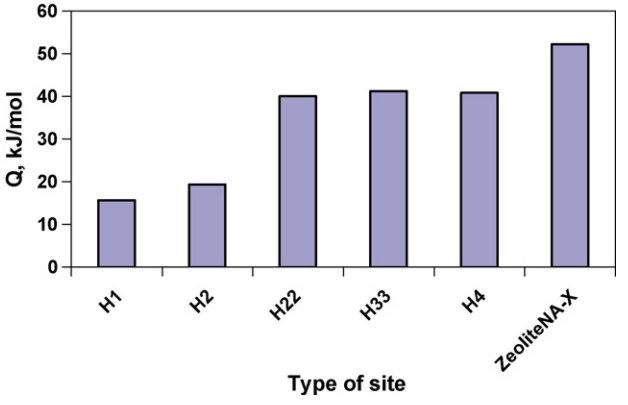

Fig. 8. Heat of adsorption, *Q*, for different hydroxyl sites at 298 K.

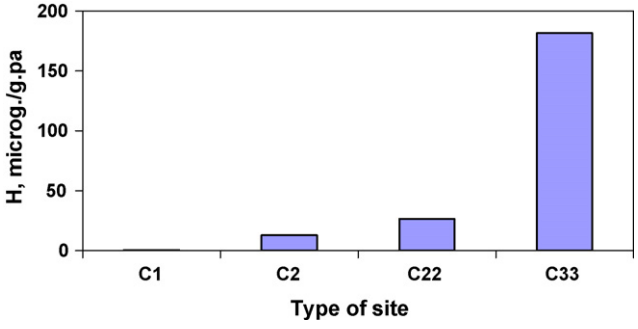

Fig. 9. Henry's law constant, *H*, for different carboxyl sites at 298 K.

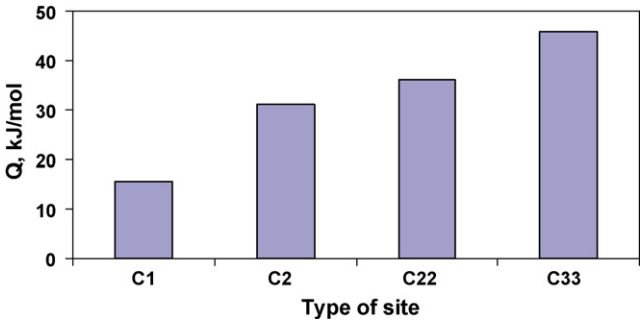

Fig. 10. Heat of adsorption, Q, for different carboxyl sites at 298 K.

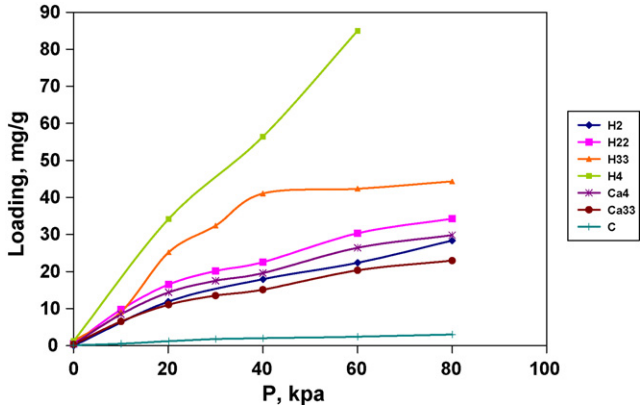

Fig. 11. Adsorption isotherms for HCN in activated carbon with hydroxyl and carbonyl sites at 298 K.

Fig. 11 indicates that the sorption capacity of the carbons with H4 and H33 were greater than with Ca33 and Ca4. Performance of H2 and H22 were found to be almost same. The higher sorption capacity of H4 and H3 can be explained from Fig. 12. The sorption in carbons with carbonyls and hydroxyls are attributed to charge–dipole and charge–induced dipole interactions. The magnitude of fluid–wall dispersion and charge–induced dipole were comparable in magnitudes. The performance of H4 and H33 was attributed to higher charge–dipole interactions.

The sorption isotherms for carboxyls and zeolite NaX indicate that zeolite NaX has the highest sorption capacity followed

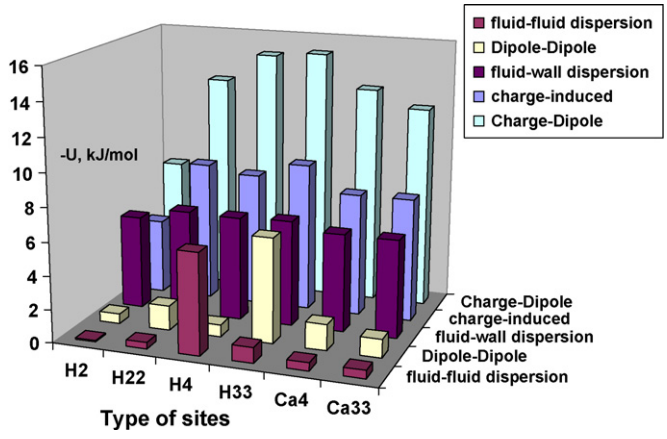

Fig. 12. Energy contributions for hydroxyl and carbonyl sites at 40 kPa and 298 K (with reference to Fig. 11).

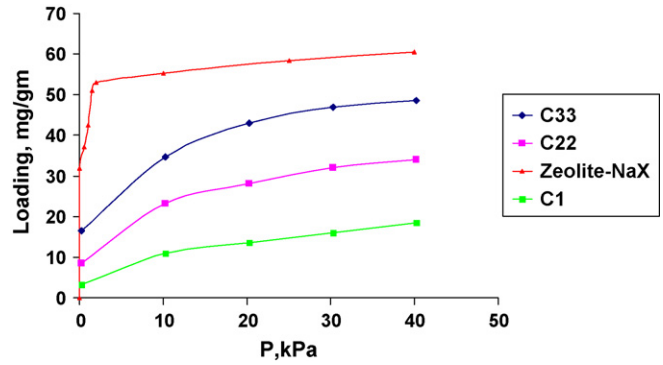

Fig. 13. Adsorption isotherms for HCN in activated carbon with carboxyl sites and zeolite NaX at 298 K.

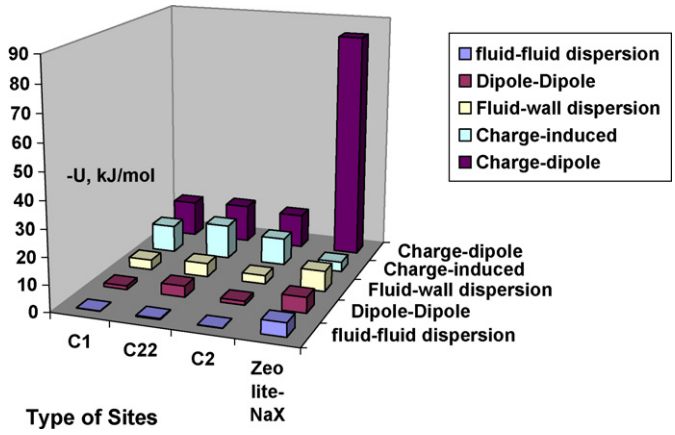

Fig. 14. Energy contributions for carboxyl sites at 40 kPa and 298 K (with reference to Fig. 13).

by C33 and C22 of activated carbons with carboxyls (Fig. 13). Fig. 14 explains that the higher sorption with pore filling in NaX is due to greater charge–dipole interactions, which is attributed to the presence of cations and the higher dipole moment of the HCN molecule (2.98 Debye). The performance of C33 and C22 was attributed to charge–dipole and charge–induced dipole interactions that were comparable in magnitudes (in the range of 15–30 kJ/mol). However, the interactions among HCN molecules were not found to be significant in carboxyls and the NaX.

4.2. Sorption of methyl ethyl ketone

Fig. 15 shows the H values for carbon with different carbonyls at 298 K, which is in the range of 1–10 μg/g Pa, whereas Q values in the range of 12–30 kJ/mol are shown in Fig. 16. H values for hydroxyls were in the range of 1–15 μg/g Pa, and Q values were in the range of 15–35 kJ/mol, however in the case of zeolite NaX. H value was 4 μg/g Pa and Q value was 12 kJ/mol (Figs. 17 and 18). The H values for carboxyls were found in the range of 3–50 μg/g Pa and Q values were in the range of 17–40 kJ/mol (Figs. 19 and 20).

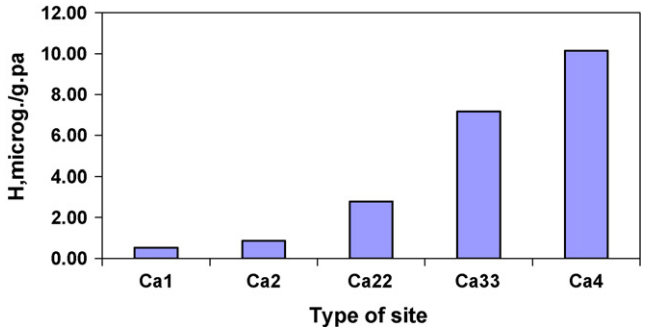

Fig. 15. Henry's law constant, H, for different carbonyl sites at 298 K.

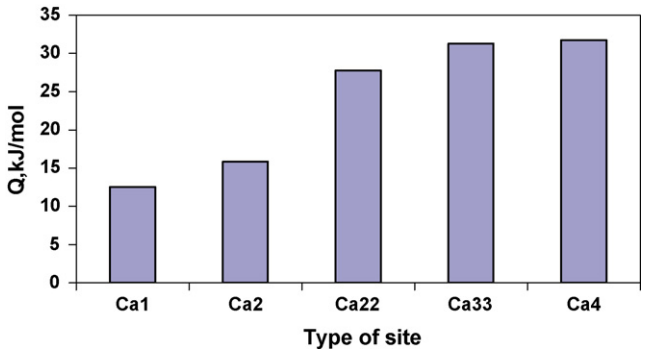

Fig. 16. Heat of adsorption, Q, for different carbonyl sites at 298 K.

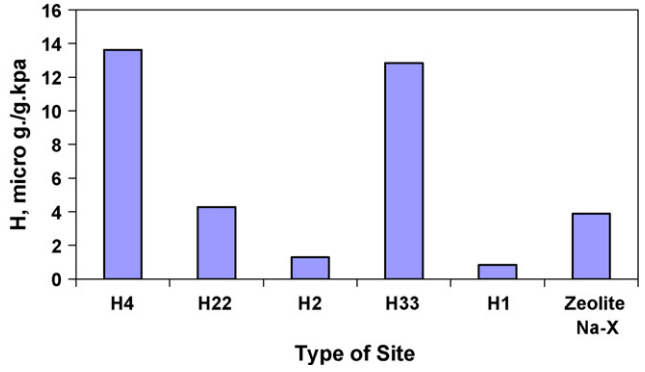

Fig. 17. Henry's law constant, H, for different hydroxyl sites at 298 K.

Fig. 21 shows the isotherms of carbon with hydroxyls, carbonyls, plain carbon (without any functional sites) and zeolite NaX. The NaX shows pore filling at low pressures, however, H33 shows more adsorption than the Ca4 carbon at pressures greater

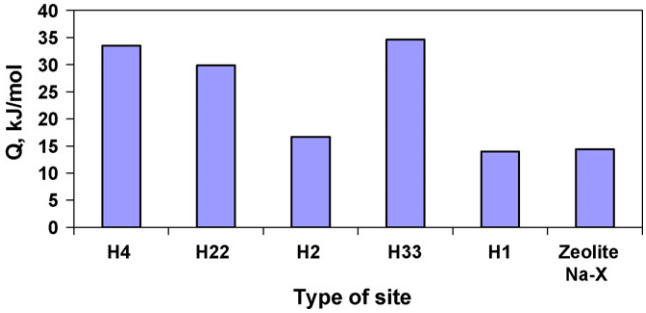

Fig. 18. Heat of adsorption, Q, for different hydroxyl sites at 298 K.

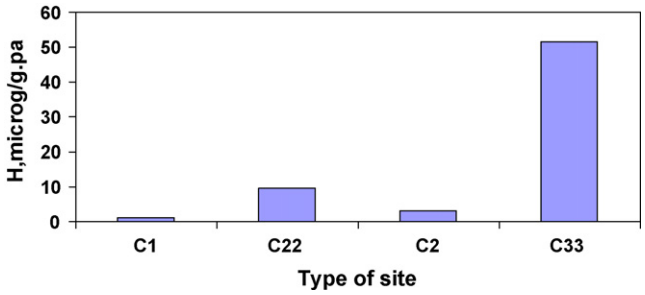

Fig. 19. Henry's law constant, H, for different carboxyl sites at 298 K.

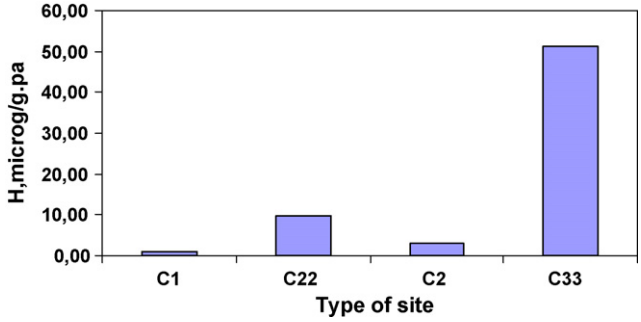

Fig. 20. Heat of adsorption, Q, for different carboxyl sites at 298 K.

than 1 kPa. Fig. 22 illustrates the magnitudes of interactions among MEK molecules, MEK-functional site (charge–induced and charge–dipole). The sudden pore filling in zeolite NaX is attributed to charge–dipole interactions (∼78 kJ/mol). The greater adsorption in the case of H33, as compared to H22 and H2, was due to higher charge–induced and fluid–wall dispersion forces.

Fig. 23 shows the adsorption isotherms for carbon with carboxyls at 298 K. Sorption in the case of C33 and C22 was above 50 mg/g for operating pressures greater than 1 kPa. This capacity is greater than that of zeolite NaX. This might be due to limited space available for MEK molecules in the spherical cavity. Fig. 24 suggests that the adsorption in the carbon with carboxyls

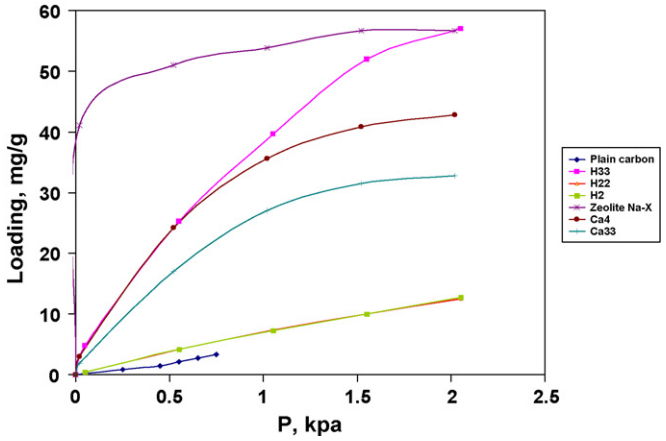

Fig. 21. MEK adsorption isotherms for carbonyl, hydroxyl, plain carbon, and zeolite NaX at 298 K.

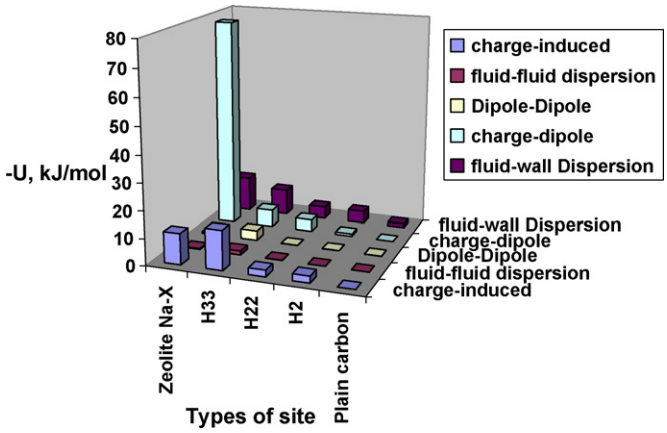

Fig. 22. Energy contributions for carbonyl, hydroxyl, plain carbon, and zeolite NaX at 2 kPa and 298 K.

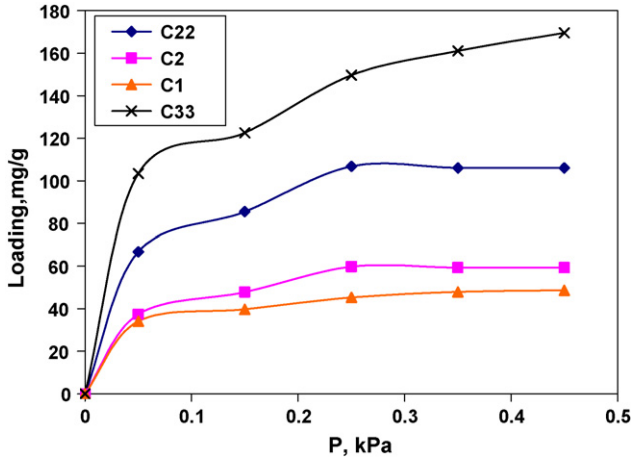

Fig. 23. Adsorption isotherms for carboxyl sites at 298 K.

is dominated by charge–induced and charge–dipole interactions. The greater magnitude of charge–induced dipole interactions is attributed to the high polarizabilty (8.12 A^3) per MEK molecule.

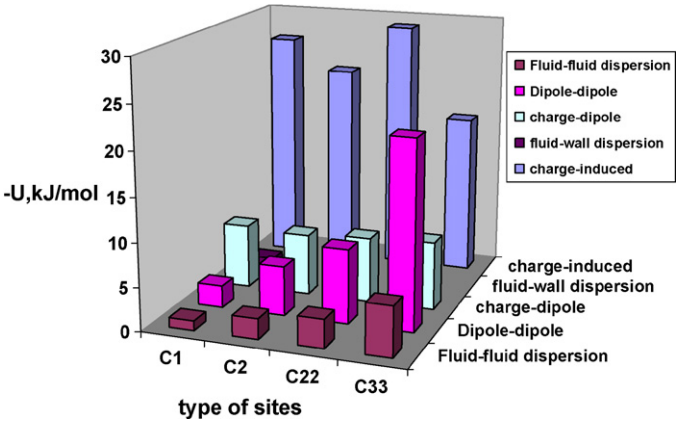

Fig. 24. Energy contributions for carboxyl sites at 0.45 kPa and 298 K.

5. Concluding remarks

In the present research study the adsorption characteristics of HCN and MEK on zeolite NaX and activated carbons with three types of acid sites were studied using GCMC simulations. On the basis of the research findings presented earlier, the following conclusions could be drawn:

1. Henry's law constant (H) and heat of adsorption (Q) values for zeolite NaX and carbons with carboxyls were greater than that of carbons with carbonyls and hydroxyls. The low affinity of the carbons with carbonyls and hydroxyls was attributed to low charge densities, and hence low electrostatic interactions with the functional groups.
2. The presence of sodium cations increases the sorption of HCN, as well as MEK, due to large Na–dipole interactions.
3. The presence of carbonyl, hydroxyl, and carboxyl sites help in increasing HCN sorption, mainly due to charge–dipole interactions that are attributed to the high dipole moment of the molecule (2.98 Debye). However, in the case of carboxyls, charge–induced and fluid–wall interactions were also significant.
4. The presence of carbonyl, hydroxyl, and carboxyl sites help in increasing MEK sorption, mainly due to charge–dipole interactions, which are attributed to the high-dipole moment of the molecule, and charge–induced dipole interactions due to the high polarizabilty of the MEK molecule.
5. Zeolite NaX shows the highest HCN adsorption with pore filling, followed by carbons with carboxyls, hydroxyls, and carbonyls, respectively, which is due to high charge densities and energetic charge–induced dipole and charge–dipole interactions for operating pressures less than 40 kPa.
6. Carbons with C33 and C22 show the highest MEK sorption, followed by carbons with C1, zeolite NaX, and carbons with hydroxyls and carbonyls, respectively, which is due to high charge densities and energetic charge–induced dipole and charge–dipole interactions for operating pressures less than 0.5 kPa. The low adsorption capacity of zeolite NaX, and sudden pore filling is attributed to limited energetic places available for MEK molecules to occupy in the spherical cavity.

References

[1] http://www.spacelab.com/compound/c78933.htm.
[2] S.H. Yen, F.T. Jeng, J. Environ. Sci. Health A 32 (8) (1997) 2087.
[3] S.W. Blocki, Environ. Prog. 12 (1993) 226.
[4] P. Monneyron, M. Manero, J. Foussard, Environ. Sci. Technol. 37 (2003) 2410.
[5] J. Pires, A. Carvalho, P. Veloso, M.B.D. Carvalho, J. Mater. Chem. 10 (2002) 3100.
[6] M.A. Uguina, J.L. Sotelo, J.A. Delgado, J.M. Gomez, L.I. Celemin, Sep. Purif. Technol. 42 (2005) 91.
[7] G.B. Freeman, P.J. Reucroft, Carbon 17 (1979) 313.
[8] P.J. Reucroft, P.B. Rao, G.B. Freeman, Carbon 21 (1983) 171.
[9] T.M. Oliver, K. Jugoslav, P. Aleksandar, D. Nikola, Chem. Eng. Proc. 44 (2005) 1187.
[10] J.L. Soto, A.L. Myers, Mol. Phys. 42 (1981) 971.
[11] F. Karavias, Ph.D. Thesis, University of Pennsylvania, 1992.

[12] R.T. Yang, Adsorbents: Fundamentals and Applications, Wiley–Interscience, New York, 2003.
[13] T.M. Reed, K.E. Gubbins, Applied Statistical Mechanics, McGraw-Hill, New York, 1973.
[14] Z. Tan, Ph.D. Thesis, Cornell University, 1992.
[15] M. Jorge, N.A. Seaton, Mol. Phys. 100 (2002) 2017.
[16] M. Jorge, C. Schumacher, N.A. Seaton, Langmuir 18 (2002) 9296.
[17] J.M. Prausnitz, R.N. Lichtenthaler, E. Gomes de Azevedo, Molecular Thermodynamics of Fluid-Phase Equilibria, 3rd ed., Prentice-Hall, NJ, 1999.